



Contents

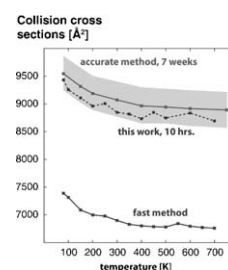
Regular Articles

1–10

A novel projection approximation algorithm for the fast and accurate computation of molecular collision cross sections (I). Method

Christian Bleiholder, Thomas Wyttenbach, Michael T. Bowers

► We develop the projected superposition approximation (PSA) to compute molecular collision cross sections measured in ion-mobility experiments. ► Molecular collision cross sections are computed as a projection approximation modified to account for collective size and shape effects. ► We show that the PSA algorithm is able to handle the geometries typical to proteins while being computationally highly efficient.

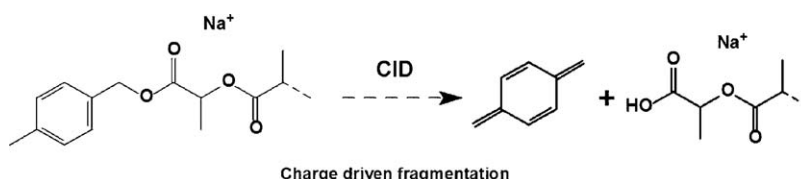


11–17

Collision-induced dissociation of polymer ions: Charge driven decomposition for sodium-cationized polylactides and isomeric end-group distinction

Julien De Winter, Olivier Coulembier, Philippe Dubois, Pascal Gerbaux

► An investigation of the CID behaviors of sodium-cationized polylactides is reported. ► Isomeric polymer ions with regioisomeric end-groups were submitted to dissociation. ► Competitive charge remote and charge driven dissociation processes were observed. ► The isomeric end-group distinction is based on the charge induced reactions.

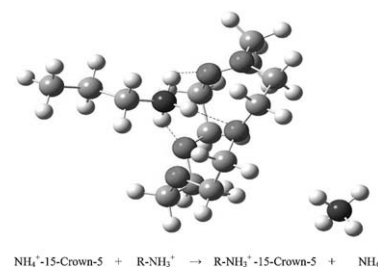


18–25

Atmospheric pressure gas-phase ammonium/alkyl ammonium exchange studies of some crown ethers complexes using ion mobility spectrometry: A thermodynamic investigation and collision cross section measurements

Naader Alizadeh, Parvin Shahdousti, Samaneh Nabavi, Mahmoud Tabrizchi

► The effect of crown ring size on the guest-exchange affinity was studied by IMS. ► The dissociation of primary crown ether-ammonium complexes is the determinant step. ► 18C6-ammonium complexes show the lowest guest-exchange affinity. ► 12C4-ammonium complexes show the highest guest-exchange affinity. ► 15C5 showed a gas phase selectivity binding to normal alkyl amine isomers.



26–34

An ion trap CIMS instrument for combined measurements of atmospheric OH and H₂SO₄: First test measurements above and inside the planetary boundary layer

Heinfried Aufmhoff, Markus Hanke, Jens Uecker, Hans Schlager, Frank Arnold

► Atmospheric OH and H₂SO₄ can be measured sensitively with an ion trap mass spectrometer. ► We developed and built a calibration source and quantified these measurements. ► Our H₂SO₄ measurements helped to get new insights into new particle formation events. ► Fragmentation of product ions verified the chemical ionization detection method.

35–40

Electron impact total ionization cross sections for H₂S, PH₃, HCHO and HCOOH

Minaxi Vinodkumar, Harshad Bhutadia, Chetan Limbachiya, K.N. Joshipura

► Electron impact ionization for simple targets (HCHO, HCOOH, PH₃ and H₂S). ► We have used improved complex scattering potential-ionization contribution (ICSP-ic) method for the calculation of Q_{ion} . ► The total inelastic cross sections (Q_{inel}) are calculated using SCOP formalism.

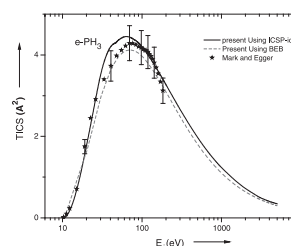


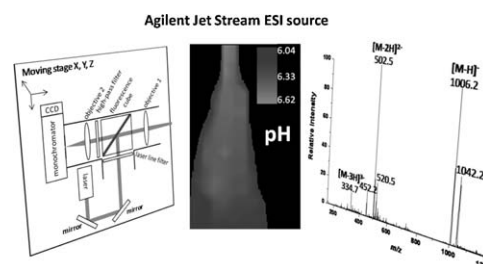
Figure: Total ionization cross sections for e- PH₃ scattering in Å².

41–48

Relation between charge state distributions of peptide anions and pH changes in the electrospray plume. A mass spectrometry and optical spectroscopy investigation

Marion Girod, Xavier Dagany, Rodolphe Antoine, Philippe Dugourd

► We couple a fluorescence set-up to an Agilent electrospray mass spectrometer. ► Investigation of the pH changes in the electrospray. ► Charge states for peptide anions are controlled by the pH of the droplets.

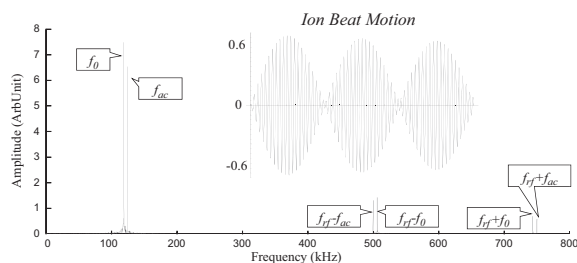


49–55

Modeling of ion transient response to dipolar AC excitation in a quadrupole ion trap

Wei Xu, William J. Chappell, Zheng Ouyang

► The initial transient stage of the ion motion in response to dipolar excitation is modeled. ► The ion motion amplitude at various frequency can be characterized. ► The ion bunching and ion beat motion phenomenon can be explained using this model.

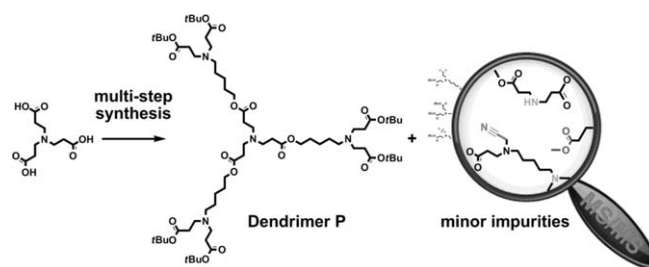


56–64

Electrospray tandem mass spectrometry of poly (amino) ester dendrimers: Dissociation rules and structural characterization of defective molecules

Aura Tintaru, Christophe Chendo, Valérie Monnier, Camille Bouillon, Gilles Quéléver, Ling Peng, Laurence Charles

► CID of poly(amino)ester dendrimer with tert-butyl terminations has been established. ► Deviation from this reference behavior allowed defective dendrimers to be characterized. ► Propagation of defects in these dendrimer synthesis could be established.

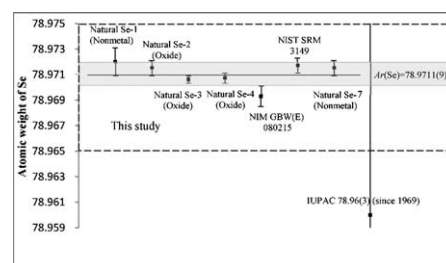


65–70

Absolute isotopic composition and atomic weight of selenium using multi-collector inductively coupled plasma mass spectrometry

Jun Wang, Tongxiang Ren, Hai Lu, Tao Zhou, Motian Zhao

► The absolute isotopic composition of Se has been determined by collision cell MC-ICP-MS in this study. Two series of synthetic isotope mixtures which gravimetrically prepared with enriched isotope materials ^{76}Se , ^{78}Se and ^{82}Se were used to correct the MC-ICP-MS. Three enriched isotope materials were further purified separately by sublimation in a specially designed vacuum vessel. Measurements of seven natural selenium samples including Se NIST SRM 3149 yielded the new atomic weight of selenium as 78.9711(9).

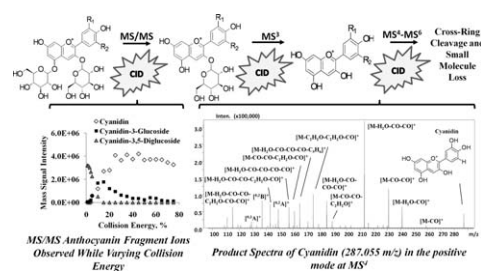


71–80

Structural characterization of cyanidin-3,5-diglucoside and pelargonidin-3,5-diglucoside anthocyanins: Multi-dimensional fragmentation pathways using high performance liquid chromatography-electrospray ionization-ion trap-time of flight mass spectrometry

Jeremy S. Barnes, Kevin A. Schug

► Anthocyanin diglucosides were identified from a rose using LC-ESI-IT-TOF-MS. ► The collision energy of the trap at each MS stage was optimized for fragmentation. ► Diagnostic fragments from cross-ring cleavage and small molecule loss were identified. ► The compounds were differentiated based on their higher order fragmentation patterns. ► A computational study was used to further characterize fragmentation.

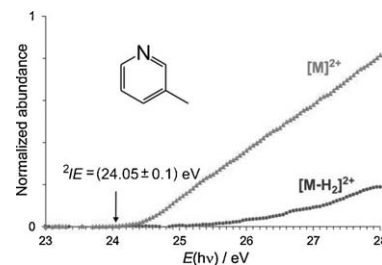


81–88

Energetics and rearrangements of the isomeric picoline dications

Lucie Ducháčková, Juraj Jašík, Ján Žabka, Daniela Ascenzi, Emilie-Laure Zins, Detlef Schröder, Stephen D. Price, Christian Alcaraz, Jana Roithová

► The double ionization threshold (2IE) for β -picoline is 24.05 ± 0.1 eV. ► 2IE of β -picoline is about 0.5 eV lower than 2IE of α - and γ -picolines. ► β -picoline dication is generated preferentially in the singlet ground state. ► α - and γ -picolines are generated as mixtures of singlet and triplet states.

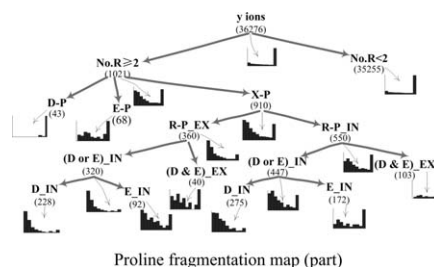


89–97

A comprehensive investigation of proline fragmentation behavior in low-energy collision-induced dissociation peptide mass spectra

Nai-ping Dong, Liang-xiao Zhang, Yi-zeng Liang

► More than 130 000 proline-containing peptides mass spectra are investigated. ► Proline effect could be suppressed by chemically driven specific effect. ► Proline effect is significantly affected by position of proline in peptides. ► New interpretation for proline effect is proposed.

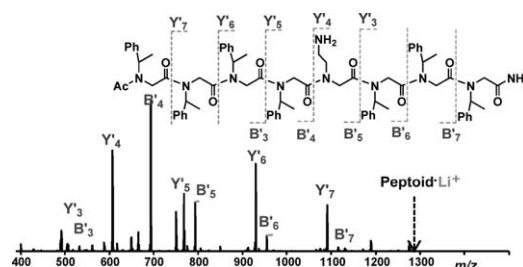


98–108

Tandem mass spectrometry studies of protonated and alkali metalated peptoids: Enhanced sequence coverage by metal cation addition

Kiran K. Morishetti, Scott C. Russell, Xiaoning Zhao, David B. Robinson, Jianhua Ren

► Charged oligo-peptoids exhibited characteristic fragmentation patterns under CID conditions. ► Protonated peptoids dissociated by producing the ions mainly retaining the C-termini. ► Alkali metalated peptoids fragmented by forming the ions with both the N- and the C-termini. ► A mobile metal cation mechanism was proposed.

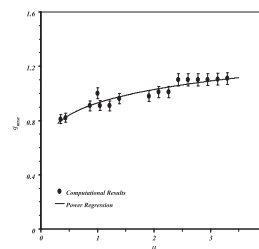


109–113

Numerical investigation of stability regions in a cylindrical ion trap

Houshyar Noshad, Behjat-Sadat Kariman

► We analyzed a cylindrical ion trap using the fifth-order Runge–Kutta (RK5) method. ► We computed three stability regions of the trap using the RK5 and RK6 techniques. ► The ratio of the area of a region for the CIT to that of a Paul trap is same. ► The effect of the trap dimensions on the first stability region was investigated. ► The area of the second region is enlarged by doubling the trap sizes.

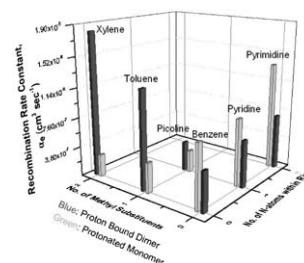


114–117

The effect of N-heteroatoms and CH₃ substituents on dissociative electron–ion recombination of protonated single six membered ring compounds at room temperature

David S. Osborne Jr, Patrick A. Lawson, Nigel G. Adams

► Protonated ring rates increase with number of nitrogens within the ring. ► Protonated ring rates decrease with the number of methyl additions. ► Proton bound ring dimers have the opposite effect of the protonated forms. ► Isomeric form has little effect on the rate.

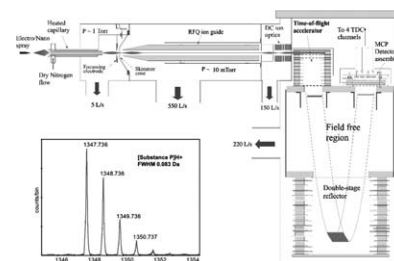


118–125

A TOF mass spectrometer for the study of noncovalent complexes

V.I. Kozlovski, L.J. Donald, V.M. Collado, V. Spicer, A.V. Loboda,
I.V. Chernushevich, W. Ens, K.G. Standing

► We have constructed a new time-of-flight mass spectrometer with ESI source. ► Accelerating voltage of 16 kV improves both transmission and detection efficiency. ► Quadrupole ion cooling and a two-stage ion mirror give mass resolution up to 18,000. ► High m/z compounds can be seen with no resolution loss at low m/z . ► The mass accuracy for noncovalent compounds is in the range of 30–40 ppm.

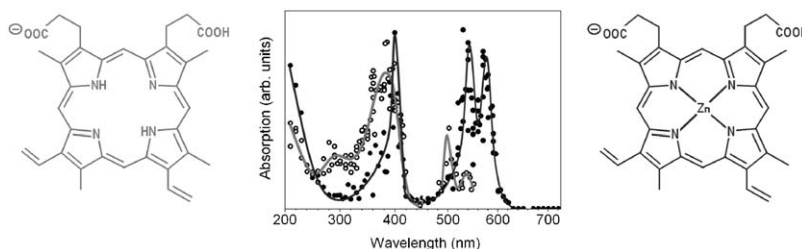


126–132

Gas-phase action spectroscopy of protoporphyrin IX (PP) and zinc-PP anions from 210 nm to 720 nm

Jean Ann Wyer, Camilla Skinnerup Jensen,
Steen Brøndsted Nielsen

► Action spectra of gas-phase protoporphyrin IX (PP) and zinc-PP anions were measured. ► The action spectra of isolated chromophores are valuable for protein biospectroscopy. ► Time spectra at each wavelength were measured. ► Absorption bands were measured at 299 nm, 386 nm, 499 nm, 535 nm and 581 nm for PP⁻. ► Absorption bands were measured at 401 nm, 542 nm and 576 nm for ZnPP⁻.

**Short communication**

133–136

Cleavage of multiple disulfide bonds in insulin via gold cationization and collision-induced dissociation

Marija Mentinova, Scott A. McLuckey

► 1 or 2 Au cations are inserted into multiply protonated insulin via ion/ion reactions. ► Incorporation of 2 Au cations leads to separation of the two chains of insulin. ► Both gold cations remain in the same chain upon separation.

